Journal of the Geological Society, London, Vol. **159**, 2002, pp. 715–729. Printed in Great Britain.

Heterogeneous exhumation in the Inner Moray Firth, UK North Sea: constraints from new AFTA® and seismic data

J. D. ARGENT[1], S. A. STEWART[2], P. F. GREEN[3] & J. R. UNDERHILL[4]

[1]*Amerada Hess Corporation, 6688 North Central Expressway, Suite 1400, Dallas, TX 75206-3925, USA (e-mail: john.argent@hess.com)*

[2]*BP, Azerbaijan, Chertsey Road, Sunbury on Thames, MIddlesex TW16 7LN, UK*

[3]*Geotrack International Pty Ltd, 37 Melville Road, West Brunswick, Vic. 3055, Australia*

[4]*Department of Geology and Geophysics, University of Edinburgh, Grant Institute, King's Buildings, West Mains Road, Edinburgh EH9 3JW, UK*

Abstract: Integration of regional seismic interpretation, sonic velocity, vitrinite reflectance and apatite fission-track analysis (AFTA®) studies has demonstrated that the western region of the Moray Firth rift arm (UK North Sea) experienced pronounced exhumation during the Cenozoic. Although this basin is usually considered to have experienced regionally uniform exhumation, interpretation of new seismic data has revealed the presence of a major system of post-Jurassic normal faults, with throws commonly in the range of 10–300 m and locally exceeding 1 km. New, high-quality seismic data are used in combination with AFTA and vitrinite reflectance data to investigate the role of extensional faulting during exhumation of this basin. Results of this interpretation not only confirm the offsets across major faults, but also show that greater exhumation and erosion occurred on their footwalls than on their hanging walls. We conclude that the localized, differential exhumation is the result of superposition of local or short-spatial-wavelength extensional tectonics upon regional, long-spatial-wavelength exhumation. These results suggest that differential exhumation might be characteristic of unroofed rift basins where normal faults subcrop the exhumation-related unconformity and that, in such cases, thermal histories from footwall locations may yield inaccurate predictions of the burial history of hanging-wall depocentres. Inaccurate burial histories will lead to a misrepresentation of the thermal history, with an impact on the estimation of hydrocarbon source rock maturity for petroleum basins.

Keywords: Moray Firth, exhumation, inversion tectonics, AFTA, source rocks.

The Moray Firth rift basin is located on the western arm of the UK North Sea Late Jurassic trilete rift system. Stratigraphic datum points in the western extremity of the Moray Firth basin, the Inner Moray Firth, are *c*. 500–1500 m shallower than they are in the Viking and Central Graben areas to the east. The shallower depth of Jurassic sediments, and the major sea-bed unconformity in the Inner Moray Firth, is generally regarded as the result of early Tertiary exhumation (Underhill 1991*a*; Hillis *et al*. 1994). (In this paper we use the term 'exhumation' to refer to height above maximum burial depth relative to the datum of present-day mean sea level.)

The deep structure of the Inner Moray Firth basin is dominated by numerous extensional tilted fault blocks that were active during the Late Jurassic synrift episode (Underhill 1991*a*). The basin's overall configuration is defined by three major fault systems; the Wick Fault on the northern margin, the Banff Fault to the south and the Helmsdale Fault to the west (Fig. 1a). Newly acquired seismic data have allowed detailed mapping of the entire basin structure bounded by these fault systems (Fig. 1a). The purpose of this paper is to integrate this new structural interpretation with direct measurements of exhumation from wells in the basin, using new apatite fission-track analysis (AFTA®) and vitrinite reflectance (VR) data obtained from deep petroleum exploration wells in the basin interior, to more fully understand the kinematics of post-Jurassic basin evolution. On the basis of these results, specifically from two exploration wells, we present here a new model of partitioned net exhumation for this basin.

Database

The seismic database consists of over 2500 km of regional 2D seismic lines. Line spacing is generally of the order of 1–2 km. Well data consist of 54 penetrations, almost all drilled to depths in excess of 2500 m (Fig. 1a). New AFTA data have been made available to this study from a number of these wells and onshore locations, but we examine in detail two offshore exploration wells, 12/23-1 and 12/24-2 (Fig. 1a). These two wells are located with 5 km separation on either side of the Smith Bank Fault and are conveniently placed to compare the exhumation on either side of this major sub-basin fault (Fig. 1a). These new offshore AFTA data were integrated with new VR measurements to give estimates of the magnitude and timing of exhumation.

Data analysis: evidence for presence, timing and magnitude of basin exhumation

Regional seismic mapping

Tilt of the whole of the western area of the North Sea is apparent from regional studies of seismic and well data (Underhill 1991a; Underhill & Partington 1993; Japsen 1997, 1999). This tilt is responsible for the relative elevation of the Inner Moray Firth rift in comparison with the deeper North Sea sub-basins further east. Sea-bed subcrop mapping within the Inner Moray Firth confirms the easterly dip of the strata (Andrews *et al*. 1990; Fig. 1a). The stratigraphic column penetrated to date by exploratory wells

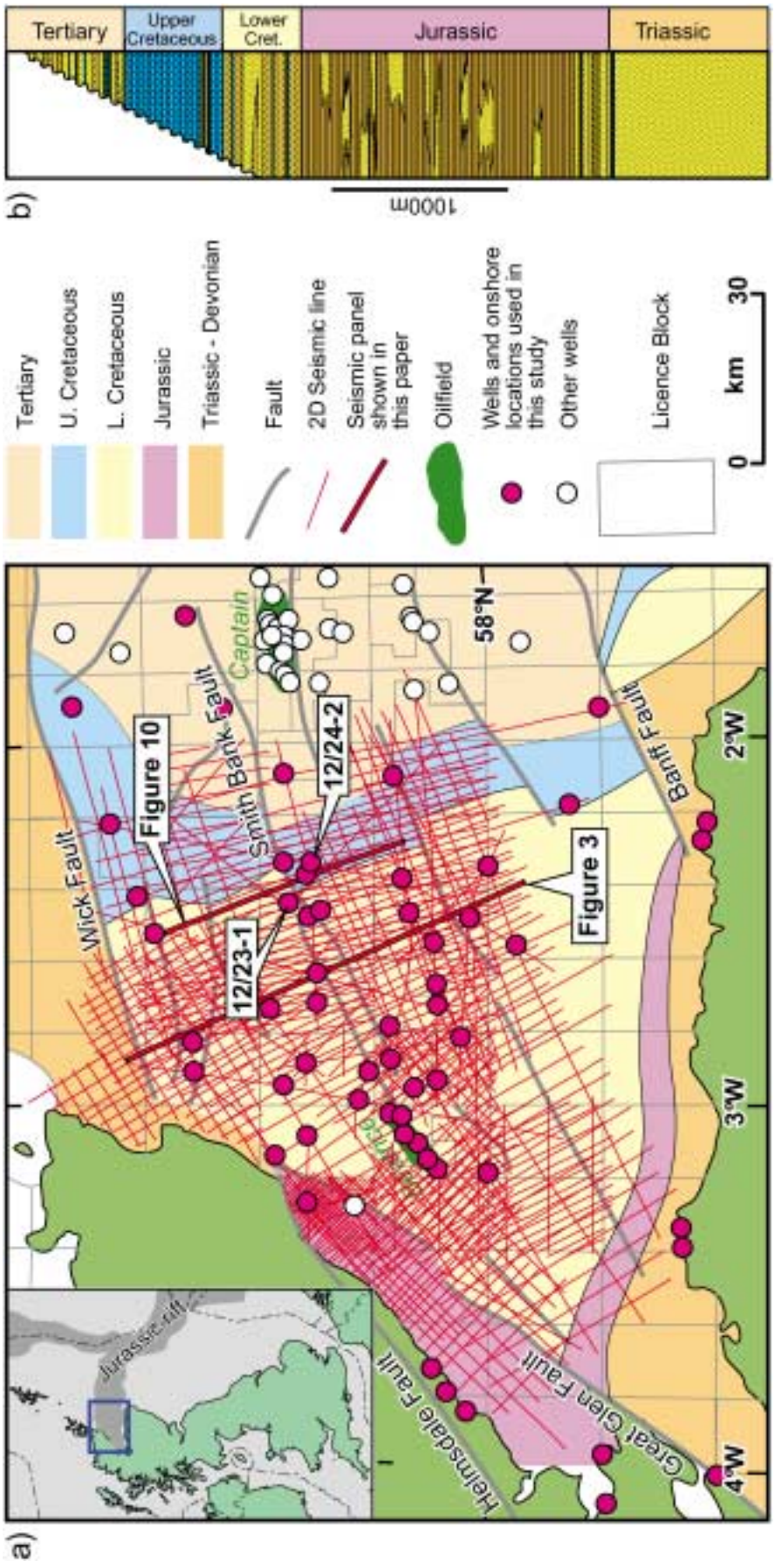

Fig. 1. (**a**) Location map of study area in the context of the North Sea rift system (Moray Firth location shown on inset map). Main map shows database of 2D seismic data and wells superimposed on map of geology at sea bed, modified in this study after Andrews *et al.* (1990). (Note the absence of Tertiary units and Chalk in the Inner Moray Firth, and the extensional faulted displacements of the base Upper Cretaceous and Base Tertiary, key evidence for significant post-Cretaceous faulting in the basin.) Key wells discussed in this paper are labelled. (**b**) Generalized stratigraphy of the Moray Firth including erosion as a result of Tertiary regional uplift in the Inner Moray Firth.

within the entire Moray Firth rift is illustrated in Fig. 1b. The complete section spans the Devonian to Tertiary. However, in the Inner Moray Firth the uppermost section of the Upper Cretaceous Chalk Group and any subsequent Tertiary sequences are absent. East–west-trending seismic lines that pass from the Inner to Outer Moray Firth show that the Upper Cretaceous Chalk Group and lowest Paleocene sediments are truncated at the sea bed, implying that exhumation began after Chalk Group deposition in the Tertiary (see fig. 4 of Argent *et al*. 2000). Argent *et al*. (2000) pointed out that the Chalk Group is the cause of many sub-Cretaceous seismic imaging problems in the North Sea, even with recent high-fidelity 3D data. Its absence from the Inner Moray Firth results in improved image quality, allowing correlations across faulted Lower Cretaceous and Jurassic sections to be made with a high degree of confidence. As indicated in Fig. 1a, most of the wells in the basin were available to this study and were used to constrain the seismic interpretation. Present-day Base Jurassic structure as mapped is shown in Fig. 2. The quality of data on which this mapping is based and the nature of the structures themselves is shown in Fig. 3, which illustrates an Upper Jurassic synrift package growing into the major extensional sub-basinal faults in the middle of the basin (Underhill 1991b). The largest faults in the Inner Moray Firth have up to 2 km offset of the Base Jurassic reflector. However, these large sub-basin bounding faults also offset the Base Cretaceous (Fig. 3) and the Base Tertiary, with throws in the range of 10–300 m. Therefore, although these structures are principally Mesozoic in age, they have a significant post-Jurassic history of reactivation that is essentially absent from the deeper North Sea sub-basins (e.g. Glennie & Underhill 1998). Some minor movement may have occurred during the deposition of the earliest Early Cretaceous, Hauterivian Stage (Fig. 3). This movement is of the order of tens of metres of displacement on the Smith Bank Fault, indicated by the minor sequence thickening towards the fault at this level. Correlation of footwall with hanging-wall reflectors suggests that subsequent Cretaceous deposition was not associated with any further extensional fault movement. The most significant component of extensional reactivation of these structures was post-Cretaceous, indicated by mapped offsets of the Top and Base Cretaceous across the main faults in the basin (Fig. 1a).

Vitrinite reflectance (VR)

A plot of VR data against depth from Inner Moray Firth exploration wells (Fig. 4) shows a wide variance of values,

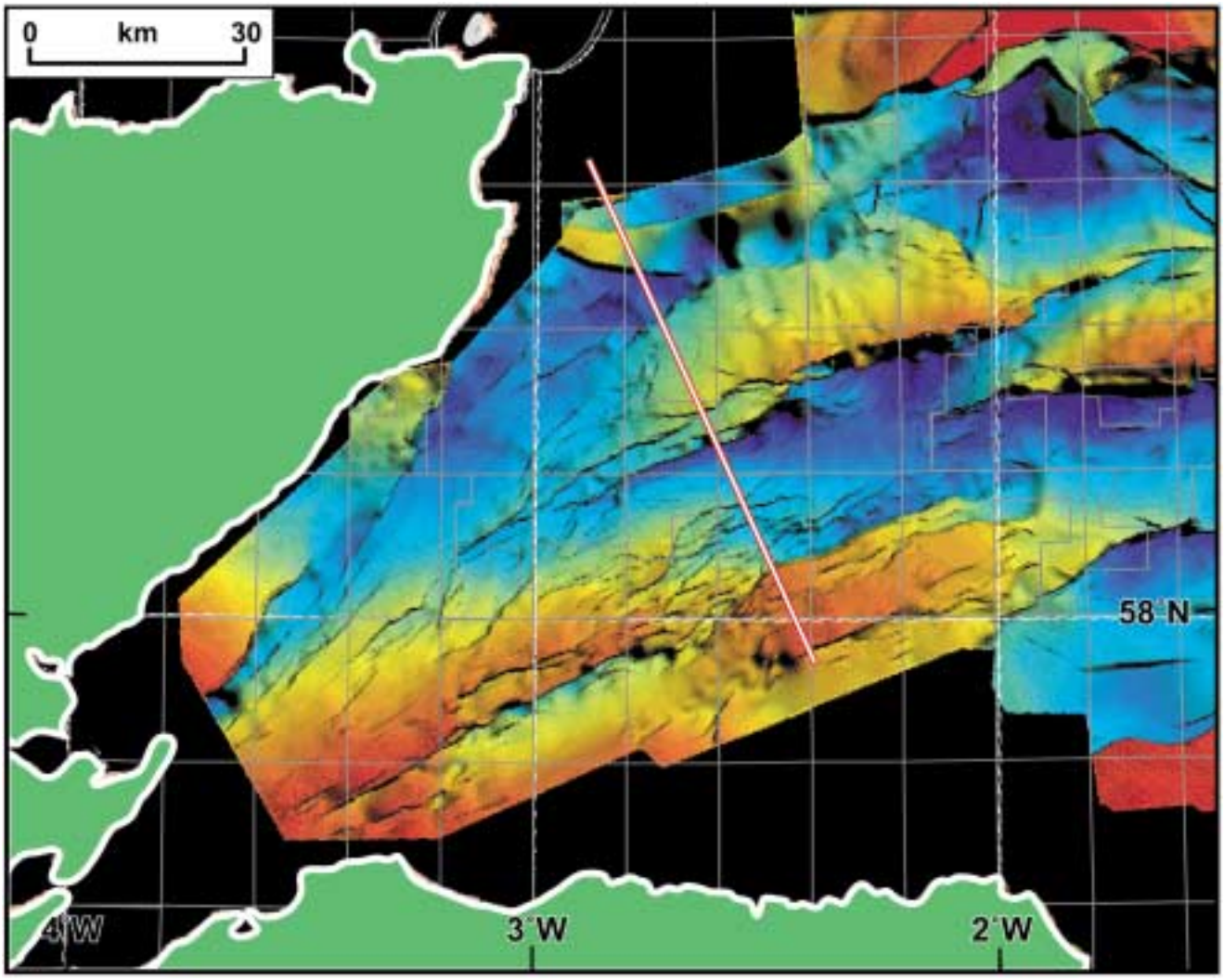

Fig. 2. Top Triassic surface within the Inner Moray Firth illustrating the well-developed post-Triassic rift architecture of the basin. Location of the seismic line shown in Fig. 3 is marked.

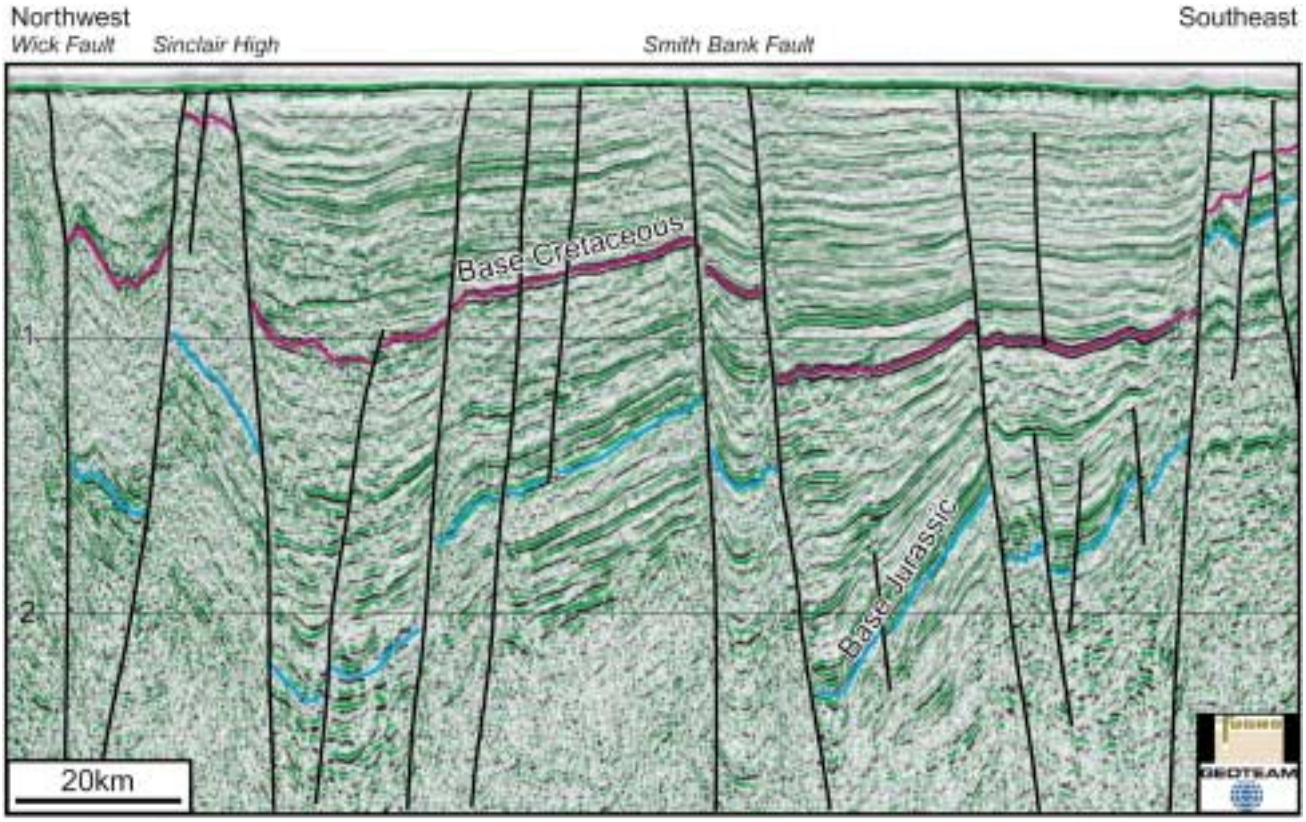

Fig. 3. Seismic section illustrating the reactivation of earlier Jurassic structures with faults subcropping the sea bed. Vertical scale is in seconds TWT (two-way travel time). Vertical exaggeration of this regional line is *c*. ×15. The largest faults in the Inner Moray Firth have up to 2 km offset of the Base Jurassic. Many faults offset the Base Cretaceous with throws in the range 10–300 m, so although these structures are principally Mesozoic in age, they have a significant post-Jurassic history of reactivation, in contrast to the deeper North Sea sub-basins. Purple horizon is Top Jurassic; blue horizon is Base Jurassic.

although individual wells exhibit consistent reflectance gradients. The vast majority of the VR data here has been determined in the organic-rich source unit of the Upper Jurassic Kimmeridge Clay Formation, often resulting in anomalously low VR estimates because of suppression effects. Unfortunately, it is not known if this combined dataset from a variety of released commercial studies consistently incorporates the variable absorption of sapropelic material within the marine clays of the Upper Jurassic shales, which may lower VR values. Large amounts of bitumen (Hutton *et al*. 1980) and oil-prone macerals (Price & Barker 1985) retard the normal increase of VR with maturity in such source shale intervals.

Notwithstanding the scatter in the dataset as a whole, the VR recorded by the majority of the wells is found to be higher than that expected for its equivalent sample depth when compared with their counterparts in the Outer Moray Firth. A reasonable explanation for this disparity is relative exhumation of the samples from the Inner Moray Firth compared with those in the Outer Moray Firth, resulting in higher apparent VR values for a given depth. In contrast, a sustained period of elevated heat flow in the region of the Inner Moray Firth would cause an offset that increases with depth. If heat flow in the region has remained close to present-day values, extrapolation of data from individual wells in Fig. 4 to surface values for unheated vitrinite (the vitrinite reflectance of wood is 0.2%) implies exhumation in the range of 500–2000 m.

Sonic velocity data

Hillis *et al*. (1994) showed that sonic velocity data for the Chalk and Kimmeridge Clay Formation shales in the Inner Moray Firth are consistent with overcompaction with respect to their present-day depth. This overcompaction suggests that these sections have been exhumed to some degree from their maximum burial depths (Fig. 5). Hillis *et al*. (1994) showed that these results contrast with those obtained from the Outer Moray Firth, where formations show no sign of overcompaction relative to their present-day depths of burial. As there is no significant change in shale composition between the Inner Moray Firth and Outer Moray Firth, such overcompaction can be explained only by exhumation of the sediments from deeper burial depths. This interpretation is in agreement with the other evidence for exhumation of the Inner Moray Firth basin discussed so far. Estimates of the amount of exhumation of individual Inner Moray Firth wells range from 580 to 1280 m. Although there was a significant spatial variation in the degree of exhumation between wells (Fig. 5), Hillis *et al*. (1994) did not attempt to relate this to the underlying basin structure.

Apatite fission-track analysis (AFTA)

AFTA is based on measurement of naturally occurring radiation damage trails or ‘fission tracks’ caused by the spontaneous fission of uranium within detrital apatite grains, which are a

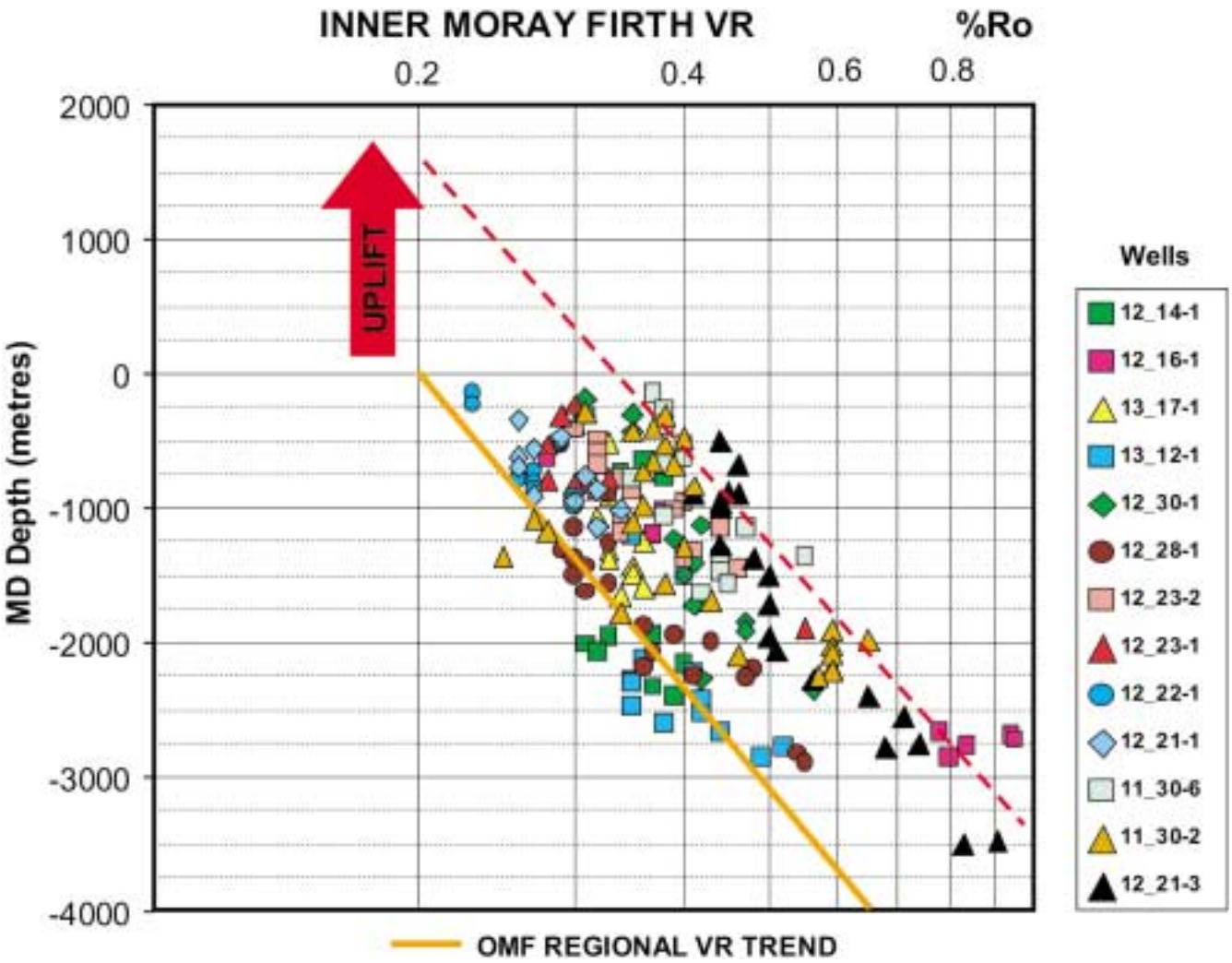

Fig. 4. VR data from Inner Moray Firth exploration wells against measured depth (MD), showing a wide variance of values, although individual wells exhibit consistent reflectance gradients. Notwithstanding the scatter in the dataset as a whole, the VR recorded by the majority of the wells is found to be higher than that expected for its equivalent sample depth when compared with their counterparts in the Outer Moray Firth (OMF). As indicated here, this can be interpreted as exhumation.

common constituent of most sandstones. The technique exploits the self-healing property of these tracks, which form at a constant rate through time and then shorten ('anneal') at a temperature-dependent rate. By measuring a 'fission-track age' (based on the number of tracks on a polished apatite grain surface) and the distribution of track lengths, it is possible to estimate the maximum palaeotemperature attained by a rock sample and the time at which the sample began to cool towards the present-day temperature. AFTA procedures and examples have been described in detail in several publications (e.g. Green *et al*. 1989a, 1989b; Bray *et al*. 1992).

The capacity of AFTA to provide an independent determination of the timing at which cooling began is particularly useful in the reconstruction of thermal and burial histories of sedimentary basins, especially if there are unconformities representing large time gaps (Duncan *et al*. 1998). In the case of the Inner Moray Firth, the Cretaceous and Tertiary sections that are present elsewhere in the North Sea are absent. Their absence is due to either exhumation and erosion of the section or non-deposition. The evidence discussed so far (seismic, VR, sonic velocity) has indicated that exhumation and erosion were responsible. AFTA provides a further, independent, means of testing this and has the potential to yield estimates of timing in addition to the magnitude of basin exhumation.

Combined AFTA and VR in the determination of exhumation magnitudes

The combined interpretation of the thermal history of both AFTA and VR data begins by assessing whether the fission-track age and track length data in each sample (and/or the VR value) could have been produced if the downhole sample had never been hotter than the present-day temperature at any time since its deposition. A burial history derived from progressively removing the overlying preserved sedimentary section is combined with the present-day geothermal gradient to construct a 'default thermal history' for each sample. Using this history, default AFTA and VR parameters can be modelled for each sample. If the observed data are consistent with the values predicted from this default history, then the sample is at or close to its maximum

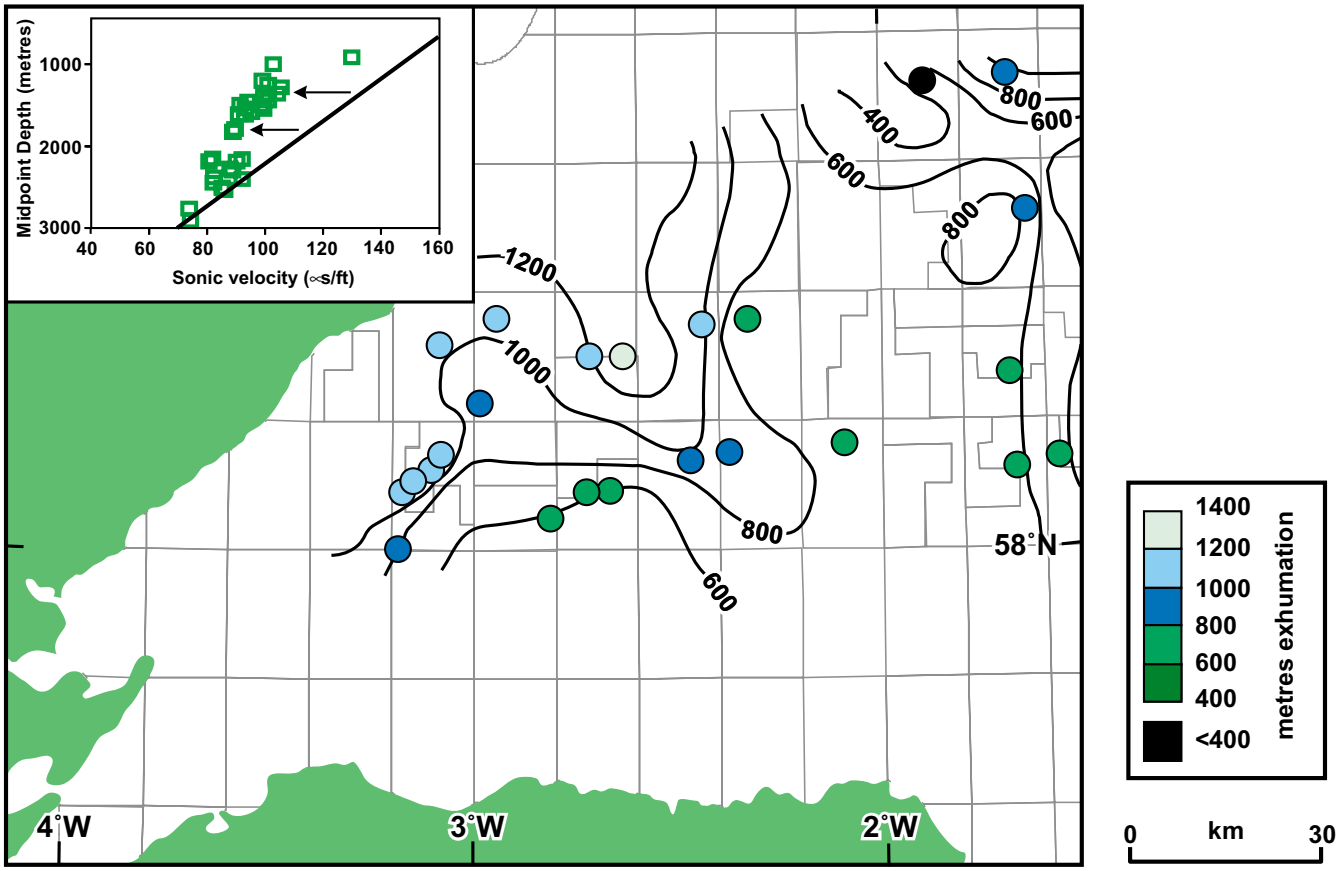

Fig. 5. Sonic log data for the Inner Moray Firth, from Hillis *et al*. (1994). Inset graph illustrates the relationship between mean sonic slowness and depth to the unit midpoint for the Kimmeridge Clay Formation. The linear normal, or undisturbed, compaction relationship is also shown. From these data Hillis *et al*. (1994) produced a total erosion map for the Inner Moray Firth reflecting the variation in exhumation across the basin (main map).

post-depositional temperature. If, however, the data show a greater degree of fission-track annealing or VR maturity than expected on the basis of this default history, the sample must have been hotter in the past than it is at the present-day depth of burial. In such cases, AFTA provides an estimate of the time at which cooling began, and both AFTA and VR constrain the magnitude of the maximum palaeotemperature reached by individual samples. Further details on the thermal history response of fission tracks in apatite, the development of AFTA parameters, and the use of AFTA and VR to extract thermal history solutions in sedimentary basins have been given by Green *et al*. (2001a, 2001b, 2002).

Analysis of samples and determination of palaeotemperatures over a range of depths within a vertical well section allows determination of the palaeogeothermal gradient at the onset of cooling. Extrapolation of the palaeogeothermal gradient to an assumed palaeo-surface temperature allows estimation of the amount of missing section (Fig. 6). This provides a measure of the magnitude of exhumation. Combining results from AFTA and VR has two advantages. First, because each technique is calibrated independently, each of the two methods provides independent verification of the results from the other. Second, the joint approach also affords the opportunity to obtain data from various lithologies through the well, to provide palaeotemperature assessment over as wide a depth interval as possible (allowing more precise constraints on palaeogeothermal gradients and removed section).

Results from two Inner Moray Firth wells

Wells 12/23-1 and 12/24-2 were selected because of their proximity to one another on adjacent margins of a major sub-basinal extensional fault (Smith Bank Fault). Well 12/23-1 is located in the footwall and 12/24-2 is located in the hanging-wall section (Fig. 1). AFTA data in six samples from these two wells are summarized in Table 1. AFTA parameters in each well (fission-track ages and mean track lengths) are plotted as a function of depth and present temperature in Fig. 7, where the fission-track age data are contrasted with the variation of stratigraphic age through the section.

Qualitative examination of the AFTA parameters from these wells shows significant contrasts that suggest major differences in the thermal history of the sequences in these two wells. For instance, fission-track ages in samples from well 12/23-1 in Fig. 7 show a more rapid decrease with depth or temperature compared with results from well 12/24-2, and at depths around 2600 m the mean track length is shorter in well 12/23-1 than in well 12/24-2.

These differences are further emphasized in Fig. 8, which shows the pattern of fission-track age v. chlorine content in sample GC237-30 from well 12/23-1 and sample GC237-55 from well 12/24-2. Most common apatites are fluorine rich; however, they may contain appreciable amounts of chlorine. The amount of chlorine in the apatite lattice exerts an important compositional control on the degree of fission-track annealing. Apatites

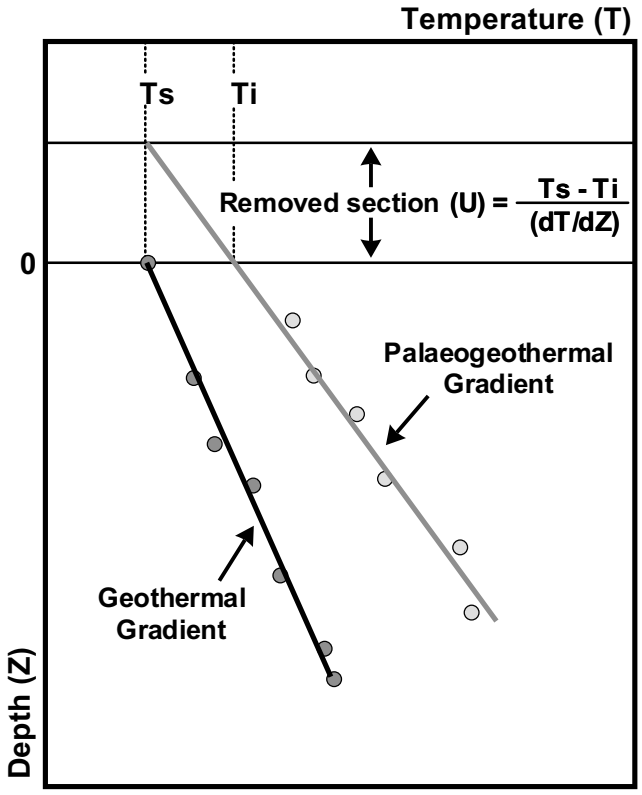

Fig. 6. Method used for the estimation of the amount of section removed with the palaeogeothermal gradient constrained by AFTA and VR, and an assumed value of surface temperature, T_s. (See Bray *et al*. (1992) for more details.)

richer in fluorine are more easily annealed than those richer in chlorine. The result of this effect is that in a single sample, individual apatite grains may show a spread in the degree of annealing. This effect becomes more pronounced at temperatures ranging from 90 to 120 °C and can therefore be useful when dealing with samples exposed to temperatures in this higher range (Green *et al*. 1996).

For each sample, the measured ages are contrasted with the pattern of age v. chlorine content predicted from the respective default thermal history for each sample. These results illustrate a key difference between the two samples, taken from present-day temperatures of 80 °C and 90 °C, respectively. Given that the default thermal histories for both samples involve residence at or above these temperatures for at least 65 Ma, representing the present-day sea-bed unconformity in each well, we might expect a slightly greater degree of annealing (age and length reduction) in sample GC237-55 (from 90 °C in well 12/24-2) compared with sample GC237-30 (from 80 °C in well 12/23-1). In fact, as the sea-bed unconformity in well 12/23-1 represents a longer interval than that in well 12/24-2, the predicted degrees of annealing are very close in the two samples despite the lower present-day temperature of GC237-30, as shown by the predicted lengths in Table 2. However, the measured data show a very different pattern. In sample GC237-30, all measured ages are much less than the values predicted from the default thermal history, showing that this sample has been hotter in the past. In contrast, measured ages in sample GC237-55 are either close to or greater than the values predicted from the default thermal history, suggesting that this sample has not been appreciably hotter than its present-day temperature at any time since deposition.

Quantitative thermal history interpretation of AFTA and VR data from these wells (following principles outlined byGreen *et al*. (2001a, 2001b, 2002)) is summarized in Table 2. This interpretation confirms the qualitative differences discussed above, and reveals further details of the thermal history of the sequences intersected in each well, as discussed in the following sections.

Well 12/23-1. Fission-track age and mean track length data were analysed for four samples at various depths within this well (Table 1). The AFTA results, taken as a whole, show that each sample has cooled from a higher temperature in the past. The evidence for this cooling event comes from the track length data in samples GC237-27, -28 and -29, which show a greater degree of reduction in track length than can be explained using the default thermal history (Table 2), and from fission-track age data in sample GC237-30, which show a greater degree of age

Table 1. *Sample details and apatite fission-track age data for samples from two Inner Moray Firth wells*

Sample number GC237-	Depth (m)	Stratigraphic details*	ρ_D† (10^6 tracks cm^2)	ρ_s† (10^6 tracks cm^2)	ρ_i† (10^6 tracks cm^2)	Zeta	Pooled/central fission-track age‡ (Ma)	$P(\chi^2)$ (%) (no. of grains)	Mean track length§ (μm)
Well 12/23-1									
27	869–905	Middle–Lower Oxfordian (157–156 Ma)	1.340 (2105)	2.074 (1181)	1.500 (854)	360.3 ± 6.8	330.8 ± 29.3	<1 (20)	11.77 ± 0.20 (101)
28	1225–1356	Upper Permian–Triassic (256–208 Ma)	1.339 (2105)	3.316 (1847)	2.613 (1455)	360.3 ± 6.8	301.9 ± 17.4	<1 (20)	11.17 ± 0.17 (103)
29	1676–1813	Lower Permian (290–256 Ma)	1.337 (2105)	2.685 (1784)	2.149 (1428)	360.3 ± 6.8	268.1 ± 22.6	<1 (20)	10.76 ± 0.20 (121)
30	2565–2566	Devonian (408–363 Ma)	1.336 (2105)	1.059 (753)	3.454 (2456)	360.3 ± 6.8	76.1 ± 10.8	<1 (20)	10.42 ± 0.24 (105)
Well 12/24-2									
55	2676–2685	Lower Volgian (152–150 Ma)	1.668 (2608)	1.144 (742)	2.757 (1789)	360.3 ± 6.8	117.2 ± 21.9	<1 (20)	8.84 ± 0.25 (110)
56	3596–3673	Triassic (208–245 Ma)	1.663 (2608)	0.563 (430)	2.074 (1583)	360.3 ± 6.8	30.6 ± 10.7	<1 (20)	9.67 ± 0.53 (27)

All analytical details are as described by Green (1986), with the exception that some thermal neutron irradiations show a significant flux gradient, in which case the appropriate value of ρ_D was determined by linear interpolation through the stack of grain mounts.

* All numerical values for stratigraphic ages assigned following Harland *et al*. (1989).

† Numbers in parentheses show the number of tracks counted in determining all track densities.

‡ Central age (Galbraith & Laslett 1993), used for samples containing a significant spread in single grain ages ($P(\chi^2)$ <5%).

§ Numbers in parentheses show the number of track lengths measured.

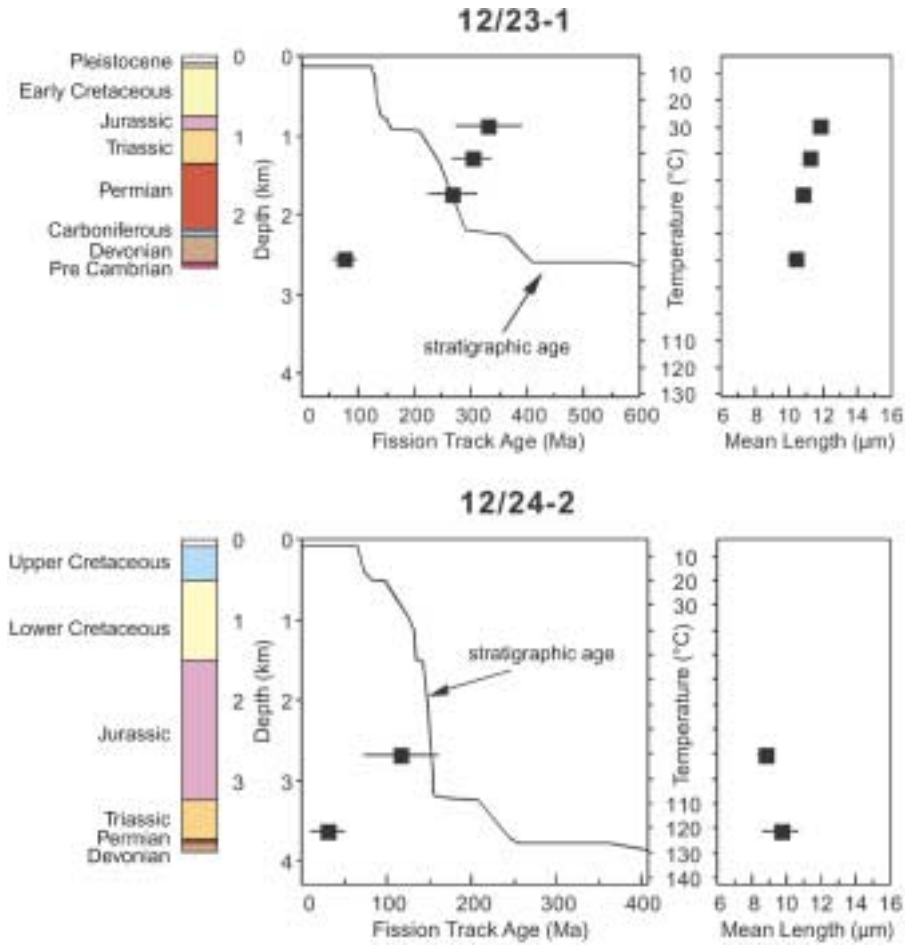

Fig. 7. AFTA parameters plotted against sample depth and present temperature for samples from wells 12/23-1 and 12/24-2. The variation of stratigraphic age with depth in each well is also shown, as the continuous line in the central panel. (See text for detailed discussion.)

reduction than can be explained by the default thermal history (Table 2 and Fig. 7).

Estimates of the magnitude of maximum palaeotemperatures and the time at which cooling from those palaeotemperatures began, derived from the AFTA data in each sample, are summarized in Table 2. Maximum palaeotemperatures increase downhole, from 65–85 °C in sample GC237-27 to >100 °C in sample GC237-30. Assuming that the data from all the samples represent a common thermal event, comparison of the timing constraints from all four samples would be consistent with a single episode of cooling beginning sometime between 100 and 40 Ma, consistent with an early Tertiary event. AFTA data from a larger number of wells in the Inner Moray Firth, also analysed as part of this study (but not fully reported here), allow this timing to be refined further to the interval 60–55 Ma, showing that the sampled units began to cool from maximum post-depositional palaeotemperatures in the Early Tertiary (Fig. 9). All the samples illustrated in Fig. 9 broadly suggest an early Tertiary age for the onset of cooling within 95% confidence limits. However, by combining the data for all the samples a refined timing of 55–60 Ma for the onset of cooling is found via overlap of the sample cooling ranges. A single sample, from well 12/29-1, is excluded from this interpretation. The onset of cooling for this sample is later, sometime between 0 and 20 Ma, and is inconsistent with that derived from all other wells and outcrop locations. Whether these data are genuine, or are some kind of analytical artefact is not known at present. On this basis, we feel that the palaeothermal effects recognized in well 12/29-1 are probably best interpreted in terms of the same Early Tertiary episode as recognized in the other samples. However, the possibility of a real difference in timing, with a later onset of cooling for the Banff High on which well 12/29-1 is located cannot be ruled out.

VR from downhole samples in well 12/23-1 are shown in Fig. 4. As summarized in Table 2, two VR values from the Barremian section and one from the Lower Permian section are higher than the values predicted by the respective default thermal history, suggesting that these units have been hotter in the past compared with their present-day temperatures. In contrast, VR values from the Upper Jurassic units in this well give anomalously low offset from the default thermal history compared with other samples from this well. This is probably due to the sapropel-rich character of the Upper Jurassic Kimmeridge Clay Formation, which is not considered to provide a reliable measurement of the true thermal maturity of this well. Maximum palaeotemperatures derived from the VR data in this well using the kinetic model of Burnham & Sweeney (1989) increase downhole from <50 °C in the Lower Cretaceous section to 92 °C in the Permian section (Table 2).

The combined palaeotemperature constraints from the VR and AFTA in well 12/23-1 are shown plotted against depth in Fig. 10a. Palaeotemperatures derived from the AFTA are consistent with those from the VR data at similar depths with the exception of the suppressed VR values obtained from the Upper Jurassic section, which are much lower than the palaeotemperatures

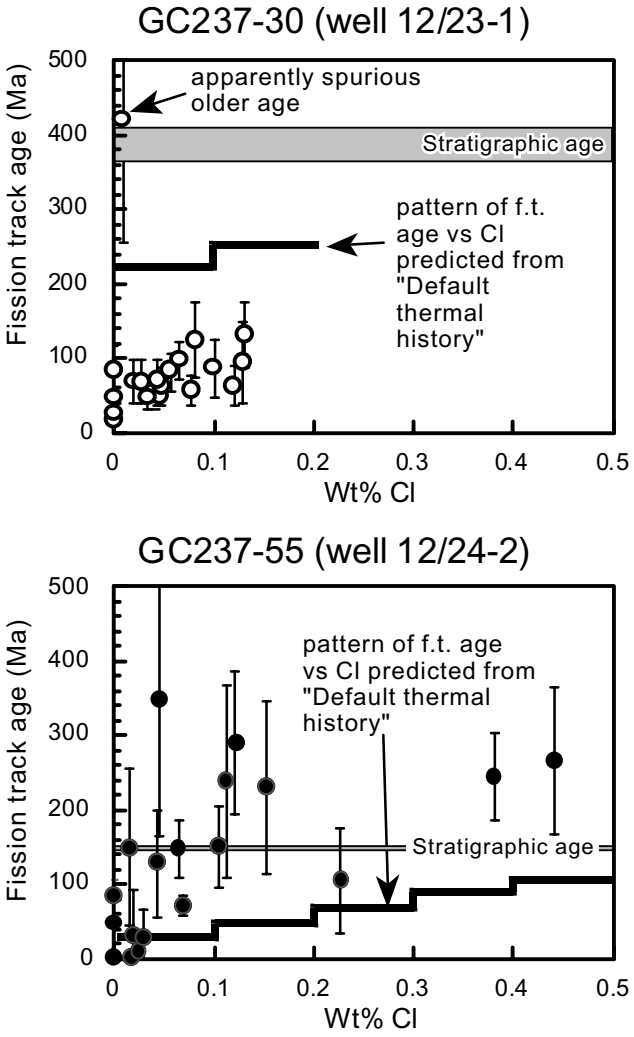

Fig. 8. Measured fission-track ages in individual apatite grains from sample GC237-30 (well 12/23-10) and sample GC237-55 (well 12/24-2), plotted against Cl content (measured by electron microprobe). Results from each sample are compared with the pattern predicted from the respective 'default thermal history', i.e. the pattern expected if the sample had not been hotter than its present temperature at any time since deposition. Measured ages in the sample from well 12/23-1 are much less than the predicted values, whereas results from well 12/24-2 are generally older than predicted. This shows that whereas the sample from well 12/23-1 has been hotter in the past, the sample from 12/24-2 is now at (or close to) its maximum post-depositional palaeotemperature.

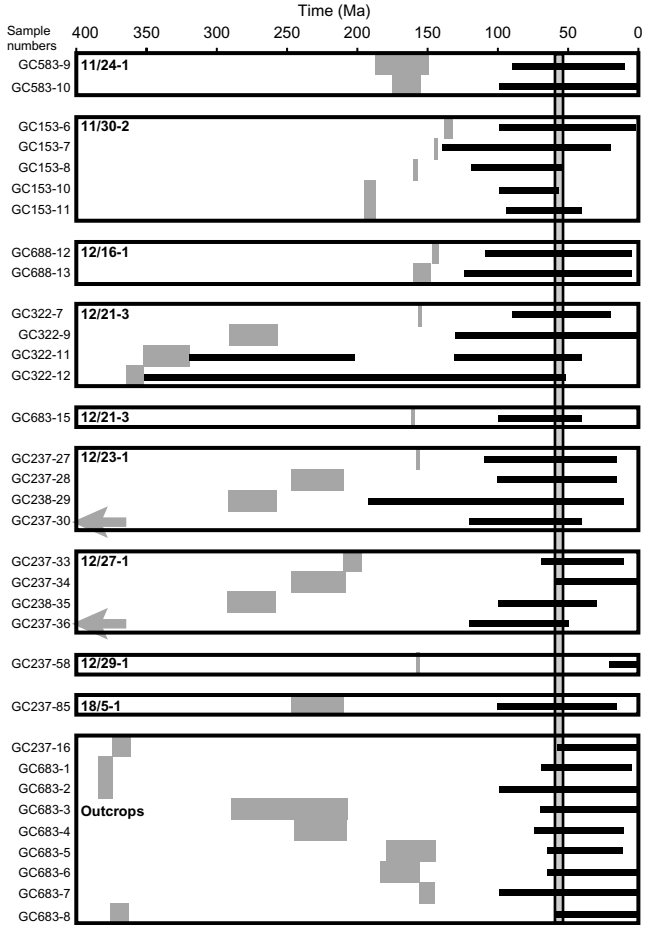

Fig. 9. Comparison of the timing information derived from AFTA data in all samples in this study, showing evidence for higher palaeotemperatures at some time after deposition. Comparison of timing in all samples suggests that cooling began between 55 and 60 Ma, as shown by the vertical green region. Grey box in each row indicates the range of depositional ages for individual samples. Black box in each row defines the range of timing for the onset of cooling derived from AFTA data in each sample within a 95% confidence interval. Vertical grey box crossing all samples shows zone of overlap of all AFTA data.

suggested by AFTA. Apart from the Upper Jurassic VR, both the AFTA and VR data therefore represent the same episode of heating.

Figure 10a shows that the AFTA and VR data both define a linear depth profile, subparallel to the present-day temperature profile but offset to a higher temperature by between 30 and 50 °C. This profile therefore suggests that the observed palaeotemperatures could be explained largely in terms of extra heating as a result of additional depth of burial, with subsequent cooling due to exhumation and erosion. The timing of this cooling event indicated by AFTA (100–40 Ma) coincides with a pronounced unconformity at a depth of 135 m in this well, across which the Barremian to Pleistocene section is absent. Therefore deeper burial, and subsequent exhumation during this interval, provides a viable explanation of the observed early Tertiary palaeotemperatures in this well.

Well 12/24-2. Results from the two AFTA samples taken from well 12/24-2 match the default thermal history predictions (Fig. 7, Table 2). The maximum limit of 125 °C set by the data from sample GC237-56 is only 4 °C above the present-day temperature of 121 °C at this depth, suggesting that only a very limited amount of additional heating may have affected this sample.

Palaeotemperature constraints from VR in this well are plotted against depth in Fig. 10b. Values derived from these VR data are lower than the present-day temperature profile. Maximum palaeotemperatures derived from the VR data vary between 69 and 95 °C, suggesting that these VR data are anomalously low; they are interpreted as having been subject to sapropelic suppression, as these samples were taken within the Upper Jurassic Kimmer-

Table 2. *Thermal history interpretation summary of AFTA and VR data in two Inner Moray Firth wells*

Sample number GC237-	Depth (m)	Stratigraphic details*	Present temperature (°C)	Default VR/ AFTA parameters†	Measured VR‡ (%)	Maximum palaeotemperature§ (°C)	Onset of cooling from AFTA (Ma)
Well 12/23-1							
	236	Middle Barremian (130–128 Ma)	11	0.27	0.30	<50	
	312	Lower Barremian (131–130 Ma)	13	0.27	0.29	<50	
	543	Lower Barremian–Hauterivian (133–131 Ma)	19	0.28	0.28	<50	
	776	Lower Valanginian (141–138 Ma)	26	0.28	0.33	50	
	792	Upper–Middle Volgian (150–146 Ma)	27	0.28	0.28	<50	
	808	Middle Volgian (152–150 Ma)	27	0.29	0.31	<50	
	823	Middle Volgian (152–150 Ma)	28	0.29	0.30	<50	
	853	Upper–Middle Oxfordian (156–155 Ma)	29	0.30	0.32	50	
27	869–905	Middle–Lower Oxfordian (157–156 Ma)	30	150 Ma 14.2 μm		65–85	100–15
28	1225–1356	Upper Permian–Triassic (256–208 Ma)	42	221 Ma 13.6 μm		75–95	100–15
29	1676–1813	Lower Permian (290–256 Ma)	55	231 Ma 12.9 μm		80–105	190–10
	1897	Lower Permian (290-256 Ma)	60	0.45	0.55	92	
30	2565–2566	Devonian (408-363 Ma)	80	229 Ma 9.9 μm		>100	120–40
Well 12/24-2							
55	2676–2685	Lower Volgian (152–150 Ma)	90	37 Ma 10.1 μm		<110	Post-deposition
	2681	Lower Volgian (152–150 Ma)	90	0.63	0.50 (30)	69	
	2856	Kimmeridgian (155–152 Ma)	96	0.66	0.55 (27)	78	
	3136	Upper–Middle Oxfordian (156–155 Ma)	105	0.73	0.67 (15)	95	
56	3596–3673	Triassic (208–245 Ma)	121	2 Ma 8.9 μm		<125	Post-deposition

* All numerical values for stratigraphic ages assigned following Harland *et al.* (1989).
† Values of vitrinite reflectance (for VR samples) or fission-track age and mean track length (for AFTA samples) predicted from the respective 'default thermal history' (as defined in the text) for each sample.
‡ Numbers in parentheses show the number of fields measured, where available.
§ Thermal history interpretation has been carried out using methods outlined by Green *et al.* (2001*a*,*b*).

idge Clay Formation. Alternatively, the present-day geothermal gradient may be lower than that used in calculating the profile. At present there is no way of discriminating between these two possibilities; however, the present-day geothermal gradient of 32.4 °C km^{-1} is comparable with that of well 12/23-1 with a present-day gradient of 29.7 °C km^{-1} taken from temperature measurements made while wireline logging of these wells was completed.

The combined results from AFTA and VR from both these downhole samples show no clear evidence of transient palaeogeothermal anomalies in the section, and the most likely explanation of the data is that all the units throughout the well are currently at or close to their maximum temperatures since deposition. We conclude that the VR results from this well consist of anomalously suppressed values, as the present-day thermal gradient of 32.4 °C km (from corrected borehole temperatures) is not unusually high and is consistent with geothermal gradients measured in other Inner Moray Firth wells.

Calculation of exhumation magnitude from wells 12/23-1 and 12/24-2

Estimates of the maximum palaeotemperatures from samples taken over a vertical depth range, such as from an exploration well, provide the capability of determining the palaeogeothermal gradient immediately before the onset of cooling. Having constrained the palaeogeothermal gradient, and assuming a value for the surface temperature at the time, the amount of section subsequently removed by exhumation and erosion can be calculated as illustrated in Fig. 6. The total amount of section removed is obtained by dividing the difference between the palaeo-surface temperature (T_s) and the intercept of the temperature profile at

Fig. 10. (**a**) Palaeotemperature constraints derived from AFTA and VR in well 12/23-1, plotted against TVDRKB (true vertical depth, below kelly bushing). Open circles show corrected BHT values. Filled circles show palaeotemperatures from VR. Horizontal bars and arrows denote palaeotemperature constraints from AFTA. The burial and exhumation history reconstruction derived from these data involves deeper burial on the post-Cretaceous unconformity in this well, with an additional 1.05-1.25 km of section removed by Tertiary exhumation and erosion. The default burial history derived from the preserved section, together with a sea-bed temperature of 6 °C and a present-day geothermal gradient of 29.7 °C km^{-1} is also shown. (**b**) Palaeotemperature constraints derived from AFTA and VR in well 12/24-2, plotted against TVDRKB. Symbols are as above. The burial and exhumation history reconstruction derived from these data shows no evidence of any palaeothermal events. Therefore this reconstruction is identical to the default burial history derived from the preserved section, together with a sea-bed temperature of 6 °C and a present-day geothermal gradient of 32.4 °C km^{-1}.

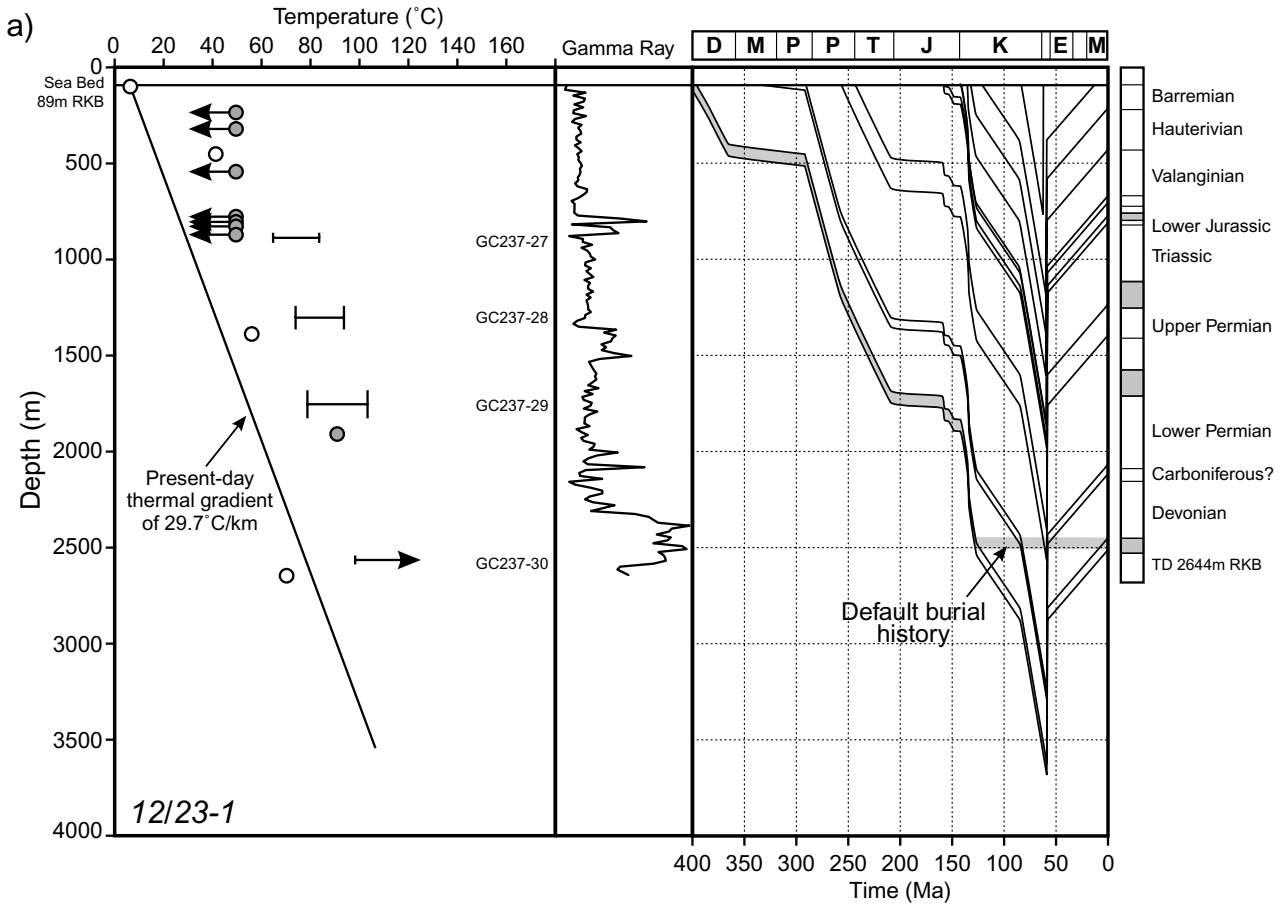
a)
Temperature (˚C)
0 20 40 60 80 100 120 140 160
Gamma Ray
D M P P T J K E M
Sea Bed
89m RKB
GC237-27
GC237-28
GC237-29
GC237-30
Present-day
thermal gradient
of 29.7˚C/km
Depth (m)
0 500 1000 1500 2000 2500 3000 3500 4000
12/23-1
Default burial
history
Barremian
Hauterivian
Valanginian
Lower Jurassic
Triassic
Upper Permian
Lower Permian
Carboniferous?
Devonian
TD 2644m RKB
400 350 300 250 200 150 100 50 0
Time (Ma)

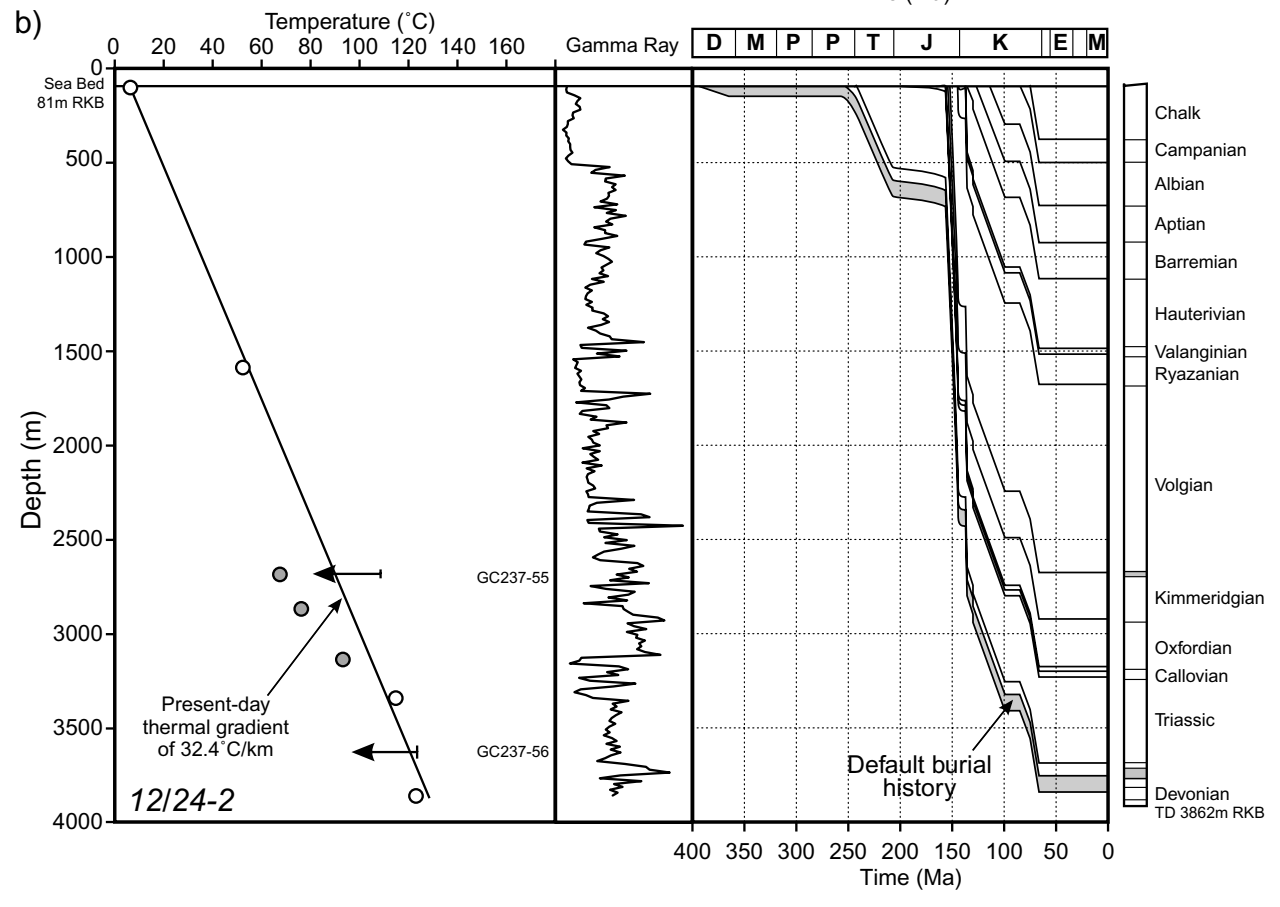
b)
Temperature (˚C)
0 20 40 60 80 100 120 140 160
Gamma Ray
D M P P T J K E M
Sea Bed
81m RKB
GC237-55
GC237-56
Present-day
thermal gradient
of 32.4˚C/km
Depth (m)
0 500 1000 1500 2000 2500 3000 3500 4000
12/24-2
Default burial
history
Chalk
Campanian
Albian
Aptian
Barremian
Hauterivian
Valanginian
Ryazanian
Volgian
Kimmeridgian
Oxfordian
Callovian
Triassic
Devonian
TD 3862m RKB
400 350 300 250 200 150 100 50 0
Time (Ma)

the appropriate unconformity (T_i) by the estimated palaeogeothermal gradient. This method relies on the assumption that the temperature profile was linear both throughout the section analysed and through the overlying section that has been removed. Consistency between estimates of eroded section derived in this way and other estimates such as seismic sections suggests that this assumption should be valid (Green *et al*. 1995).

The calculated Early Tertiary palaeotemperature profile in well 12/23-1 is linear and subparallel to the present-day temperature profile (with a gradient of *c*. 30 °C km in each case), supporting the evidence discussed above that heating was mainly due to additional depth of burial (with subsequent cooling as a result of exhumation) rather than elevated, transient heat flow. An estimate of the thickness of section eroded from the sea-bed unconformity can be made by making a linear extrapolation of the present-day and palaeogeothermal gradients to a surface temperature of 6 °C. This method yields 1.05–1.25 km of missing section from well 12/23-1.

In contrast, results from well 12/24-2 do not require any appreciable amount of eroded section. This indicates a significant variation in the amount of exhumation between these two wells, in spite of their limited spatial separation (5 km). However, the wells lie either side of the Smith Bank Fault, a major normal fault that is seen to have a history of post-Jurassic extensional movement on seismic data. A possible alternative interpretation is that the palaeogeothermal gradient in well 12/24-2 could have been underestimated, such that the section was hotter in the past, therefore allowing some degree of Tertiary exhumation and erosion. However, the amounts of removed section must be fairly small as the Chalk Group is still present in the shallow section of the well and some degree of structural control would still be required to explain the differences in thickness of the preserved section between the two wells.

Integration of AFTA and VR results with seismic imaging of Smith Bank Fault

A seismic line tying wells 12/23-1 and 12/24-2 illustrates the post-Jurassic history of extensional movement on the Smith Bank Fault (Fig. 11). Mapping of the whole dataset (Fig. 1a) shows that most of this displacement is post-Cretaceous. The depths to Base Jurassic and Base Cretaceous in the wells, tied to the seismic image, indicate that there has been 2350 m of post-Triassic displacement on the Smith Bank Fault, of which 750 m is post-Jurassic. Uncertainty in these estimates arises principally from seismic time to depth conversion away from the well control and we estimate that the error in these measurements is $<$30 m. Differential burial between these two wells was estimated at 670 m in the sonic velocity study of Hillis *et al*. (1994) at the level of the Base Cretaceous. This burial estimate is comparable with the integrated AFTA and VR data results obtained in this study, which additionally suggest that cooling commenced at 55–60 Ma. Although the thermal history reconstruction may have marginally overestimated the amount of exhumation, the results from this integrated AFTA and VR study may be indicative of uncertainty in the palaeogeothermal gradi-

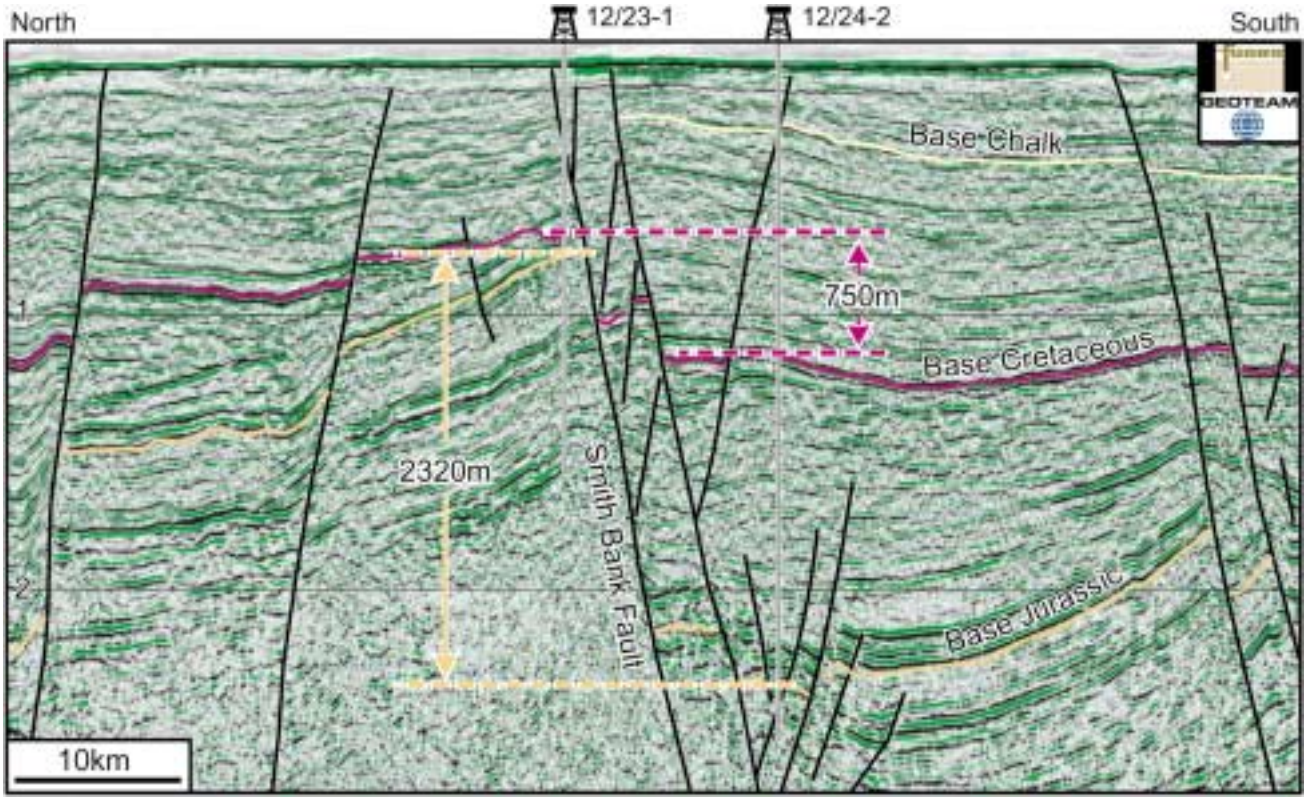

Fig. 11. A seismic line tying wells 12/23-1 and 12/24-2 clearly shows a post-Jurassic history of extensional movement on the Smith Bank Fault. Annotation as in Fig. 3. Vertical exaggeration of this line is *c*. ×9. The depths to Base Jurassic and Base Cretaceous in the wells, tied to the seismic image with well control, indicate that there has been 2350 m of post-Triassic displacement on the Smith Bank Fault, of which 750 m is post-Jurassic. The AFTA and VR estimates of differential exhumation between these two wells in this study, and those of Hillis *et al*. (1994), are consistent with the seismically observed post-Jurassic offset of 750 ± 30 m.

ent estimation. In addition, results from well 12/24-2 would allow a small amount of removed section in that well, with cooling of 5–10 °C equivalent to *c*. 150–300 m of missing section, which could not be resolved within the palaeotemperature data (as the Chalk Group subcrops at the sea bed in the location of well 12/24-2, some degree of erosion must have occurred at this site). These independent estimates of exhumation are all consistent with the seismically observed post-Jurassic offset of 750 ± 30 m. Most of these large sub-basinal bounding faults in the Inner Moray Firth exhibit some degree of post-Jurassic fault reactivation (Fig. 1), and similar to the Smith Bank Fault, these faults are truncated at the sea bed.

Kinematics of basin exhumation

Here we synthesize the observations and interpretations presented so far into a tectonic model representing basin exhumation. Rather than choose a specific model straight away, we first define three end-member kinematic options, each model characterized by various combinations of regional exhumation (on a wavelength of hundreds of kilometres) and fault tectonics (Fig. 12). The effects of the end-member models are depicted in relation to an initial rift basin template (Fig. 12a) that is intended to represent the geometry of the Inner Moray Firth at the end of the Cretaceous. In the following discussion we choose a preferred model.

The first possibility shown in Fig. 12b has little or no contribution from intra-basinal faulting during regional uplift and can be termed epeirogenic exhumation (Hallam 1963; McKenzie 1984). Epeirogenic exhumation would lead to smooth, progressive variations in exhumation of flat, regional stratigraphic markers (Fig. 12b), as noted elsewhere on the Atlantic margins (e.g. Pazzaglia & Gardner 1994; Rohrman & van der Beek 1996). The spatial variations in the amount of exhumation suggested by previously published studies (Hillis *et al*. 1994) and confirmed by the investigation of the Smith Bank Fault presented here, suggest that local, differential exhumation has been important and we rule out epeirogenic exhumation as shown in Fig. 12b as the single mechanism responsible for basin exhumation of the Inner Moray Firth.

At the other extreme, reverse faulting could cause the pattern of exhumation and basin inversion. The differential exhumation of well 12/23-1 relative to well 12/24-2 could be accounted for if well 12/23-1 lay in an overthrust block. This defines a second kinematic possibility of basin-wide inversion controlled by reverse reactivation of extensional faults, with or without a background signature of epeirogenic exhumation, giving a heterogeneous picture of basin inversion (Fig. 12c) and perhaps better accounting for the rapid local variations in degree of exhumation suggested by various Inner Moray Firth studies. This type of heterogeneous inversion occurred during the Cretaceous and Tertiary on the south margin of the southern North Sea (Badley *et al*. 1989). However, the seismic data (Figs. 3 and 11) clearly show that the Smith Bank Fault is an extensional fault dipping to the SE and not a reverse fault dipping to the NW as required by the well 12/23-1 data. We rule out this option because of the incompatibility between the kinematics of this model and the data.

A third kinematic model combines a background of regional exhumation accompanied by extensional faulting (Fig. 12d). The displacement across extensional faults is usually partitioned *c*. 17:3 between hanging-wall subsidence and footwall exhumation relative to local datum points (Jackson *et al*. 1988; Gibson *et al*. 1989). However, if the entire area that is being extensionally faulted is simultaneously regionally exhumed, the net movement of hanging wall and footwall relative to regional datum points will be a function of both processes. Both sides of the extensional fault may become exhumed relative to regional datum points, in spite of extension across the fault (Fig. 12d). Downthrow of the hanging wall is essentially buffered by the regional exhumation. We propose that this third kinematic model accounts for the spatial variation in exhumation observed in the various lines of evidence from Inner Moray Firth presented in this paper. This model accounts for the curious phenomenon of wells in hanging-wall lows exhibiting conventional, non-exhumed thermal histories whereas adjacent wells on footwalls highs can show significant amounts of exhumation. The model reconciles documented regional uplift of the west margin North Sea basin (Rohrman & van der Beek 1996; Japsen 1997) and

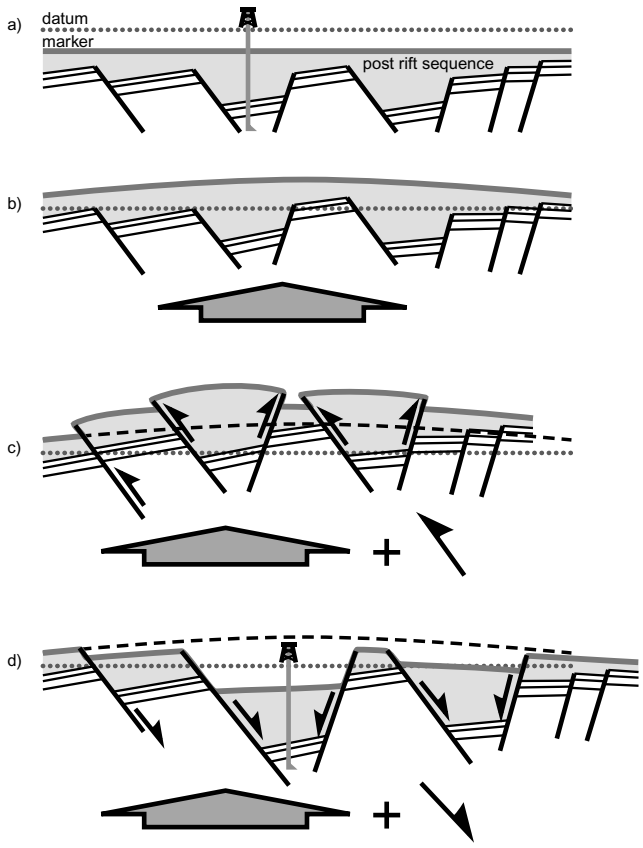

Fig. 12. Three end-member kinematic models that could account for basin exhumation. These models are characterized by various combinations of regional exhumation (on a wavelength of hundreds of kilometres) and fault-controlled differential local exhumation. (**a**) Notional rift basin template. (**b**) Exhumation with little or no contribution from intra-basinal faulting during regional exhumation, termed epeirogenic. (**c**) Basin-wide inversion controlled by numerous reverse faults, which give a heterogeneous picture of basin inversion, combined with some contribution of regional exhumation (the same amount as shown in (**b**)). (**d**) Regional exhumation accompanied by extensional faulting. Both sides of the extensional fault may become exhumed relative to regional datum points, in spite of the extension across the fault. Downthrow of the hanging wall is essentially buffered by the regional exhumation. It should be noted that the stratigraphy and burial history encountered in the highlighted hanging-wall well are essentially the same as in the non-inverted scenario shown in (**a**).

post-Jurassic basement-linked extensional fault reactivation, which although restricted to the Inner Moray Firth (Underhill 1991a, 1998; Stewart 1996) has also been identified in the Bressay area of the East Shetland Basin (Underhill 2001). It should be noted that in adopting this model we do not suggest any genetic link between the regional exhumation and the extensional faulting in the Inner Moray Firth. The Cenozoic extensional faulting in the Inner Moray Firth basin demonstrated here may also have occurred onshore and contributed displacement to fault contacts in the deeply eroded basement of the Scottish Highlands (see Roberts & Holdsworth 1999 and Thomson *et al*. 1999).

This model of heterogeneous finite exhumation has implications for petroleum systems modelling. If, for example, all the well data were confined to penetrations into the footwall highs within this basin, as is often the case in the early phases of hydrocarbon exploration, the magnitude of hanging-wall burial might have been overestimated. This overestimate might result from projecting a missing or condensed section observed in the wells drilled into structural traps on the footwall highs into pseudo-wells used to model burial history of the hanging-wall lows. Modelling the basin in such a way would lead to an erroneous estimate of kerogen maturity within the hydrocarbon kitchen areas.

The net result of the tectonic model described in this paper is partitioning of exhumation across extensional faults. It is not known at present how extensive this phenomenon is along the western margin of the North Sea, or the eastern margin of the Atlantic. However, it is possible that this effect may be found wherever Mesozoic faults are exhumed to the sea bed or surface, and exhumation data measured in adjacent fault blocks should be projected across these faults with some circumspection.

Conclusions

A synthesis of seismic, apatite fission-track analysis and vitrinite reflectance data from the Inner Moray Firth Basin shows significant local variations in Cenozoic exhumation across extensional faults. We account for these observations with a kinematic model of differential basin exhumation consisting of superposition of regional, epeirogenic exhumation, and local, short-wavelength extensional faulting. Although the hanging wall of the extensional faults is of same order as the degree of 'regional' exhumation, the true nature and extent of 'basin inversion' appears to have been recorded only in their footwalls.

The views expressed here are solely those of the authors and do not necessarily represent those of the Amerada Hess Corp., BP Plc or Geotrack International Pty Ltd or any associated partner companies. AFTA® is a registered trademark owned and maintained by Geotrack International Pty Ltd. We are grateful to P. Broad of Fugro Geoteam A/S for permission to show examples of recent seismic data from the region, and C. Tannock of Talisman Energy UK Ltd for permission to publish the AFTA data. This manuscript benefited from thorough review and helpful advice from J. Cartwright (Cardiff University) and J. Turner (Birmingham University).

References

Andrews, I.J., Long, D., Richards, P.C., Thomson, A.R., Brown, S., Chesher, J.A. & McCormac, M. 1990. *United Kingdom Offshore Regional Report: the Geology of the Moray Firth.*. HMSO, HMSO, London.

Argent, J.D., Stewart, S.A. & Underhill, J.R. 2000. Controls on the Lower Cretaceous Punt Sandstone Member, a massive deep-water clastic deposystem, Inner Moray Firth, UK North Sea. *Petroleum Geoscience*, **6**, 275–285.

Badley, M.E., Price, J.D. & Backshall, L.C. 1989. Inversion, reactivated faults and related structures: seismic examples from the southern North Sea. *In:* Cooper, M.A. & Williams, G.D. (eds) *Inversion Tectonics*. Geological Society, London, Special Publications, **44**, 201–219.

Bray, R.J., Green, P.F. & Duddy, I.R. 1992. Thermal history reconstruction using apatite fission track analysis and vitrinite reflectance: a case study from the U.K. East Midlands and southern North Sea. *In:* Hardman, R.F.P. (ed.) *Exploration Britain: Geological Insights for the Next Decade*. Geological Society, London, Special Publications, **67**, 3–25.

Burnham, A.K. & Sweeney, J.J. 1989. A chemical kinetic model of vitrinite reflectance maturation. *Geochimica et Cosmochimica Acta*, **53**, 2649–2657.

Duncan, W.I., Green, P.F. & Duddy, I.R. 1998. Source rock burial history and seal effectiveness: key facets to understanding hydrocarbon exploration potential in the east and central Irish Sea Basins. *AAPG Bulletin*, **82**, 1401–1415.

Galbraith, R.F. & Laslett, G.M. 1993. Statistical methods for mixed fission track ages. *Nuclear Tracks*, **21**, 459–470.

Gibson, J.R., Walsh, J.J. & Watterson, J. 1989. Modelling of bed contours and cross-sections adjacent to planar normal faults. *Journal of Structural Geology*, **11**, 317–328.

Glennie, K.W. & Underhill, J.R. 1998. The development and evolution of structural styles in the North Sea. *In:* Glennie, K. (ed.) *Introduction to the Petroleum Geology of the North Sea*, *4th*. Blackwell Science, Oxford, 42–84.

Green, P.F. 1986. On the thermo-tectonic evolution of Northern England: evidence from fission track analysis. *Geological Magazine*, **123**, 493–506.

Green, P.F., Duddy, I.R. & Bray, J.R. 1995. Applications of thermal history reconstruction in inverted basins. *In:* Buchanan, J.G. & Buchanan, P.G. (eds) *Basin Inversion*. Geological Society, London, Special Publications, **88**, 149–165.

Green, P.F., Duddy, I.R., Bray, R.J., Duncan, W.I. & Corcoran, D. 2001b. Thermal history reconstruction in the Central Irish Sea Basin. *In:* Shannon, P.M., Haughton, P.M. & Corcoran, D. (eds) *Petroleum Exploration of Ireland's Offshore Basins*. Geological Society, London, Special Publications, **188**, 171–188.

Green, P.F., Duddy, I.R., Gleadow, A.J.W. & Lovering, J.F. 1989a. Apatite fission track analysis as a palaeotemperature indicator for hydrocarbon exploration. *In:* Naeser, N.D. & McCulloh, T. (eds) *Thermal History of Sedimentary Basins—Methods and Case Histories*. Springer, New York, 181–195.

Green, P.F., Duddy, I.R. & Hegarty, K.A. 2002. Quantifying exhumation in sedimentary basins of the UK from apatite fission track analysis and vitrinite reflectance data: precision, accuracy and latest results. *In:* Doré, A.G., Cartwright, J.A., Stoker, M.S., Turner, J.P. & White, N.J. (eds) *Exhumation of the Circum-Atlantic Margins*. Geological Society, London, Special Publications, **xx**, xxx–xxx.

Green, P.F., Duddy, I.R., Laslett, G.M., Hegarty, K.A., Gleadow, A.J.W. & Lovering, J.F. 1989b. Thermal annealing of fission tracks in apatite 4. Quantitative modelling techniques and extension to geological timescales. *Chemical Geology (Isotope Geoscience Section)*, **79**, 155–182.

Green, P.F., Hegarty, K.A. & Duddy, I.R. 1996. Compositional influences on fission track annealing in apatite and improvement in routine application of AFTA. *American Association of Petroleum Geologists, Abstracts with Program*, A56.

Green, P.F., Thomson, K. & Hudson, J.D. 2001a. Recognising tectonic events in undeformed regions: contrasting results from the Midland Platform and East Midlands Shelf, Central England. *Journal of the Geological Society, London*, **158**, 59–73.

Hallam, A. 1963. Major epeirogenic and eustatic changes since the Cretaceous, and their possible relationships to crustal structure. *American Journal of Science*, **261**, 397–423.

Harland, W.B., Armstrong, R.L., Cox, A.V., Craig, L.E., Smith, A.G. & Smith, D.G. 1989. *A Geologic Time Scale 1989*. Cambridge University Press, Cambridge University Press, Cambridge.

Hillis, R.R., Thomson, K. & Underhill, J.R. 1994. Quantification of Tertiary erosion in the Inner Moray Firth using sonic velocity data from the Chalk and the Kimmeridge Clay. *Marine and Petroleum Geology*, **11**, 283–293.

Hutton, A.C., Kantsler, A.J., Cook, A.C. & McKirdy, D.M. 1980. Organic matter in oil shales. *Journal of the Australian Petroleum Exploration Association*, **20**, 44–67.

Jackson, J.A., White, N.J., Garfunkel, Z. & Anderson, H. 1988. Relations between normal-fault geometry, tilting and vertical motions in extensional terrains: an example from the southern Gulf of Suez. *Journal of Structural Geology*, **10**, 155–170.

Japsen, P. 1997. Regional Neogene exhumation of Britain and the western North Sea. *Journal of the Geological Society, London*, **154**, 239–247.

Japsen, P. 1999. Overpressured Cenozoic shale mapped from velocity anomalies relative to a baseline for marine shale, North Sea. *Petroleum Geoscience*, **5**, 321–336.

McKenzie, D. 1984. A possible mechanism for epeirogenic uplift. *Nature*, **307**, 616–618.

Pazzaglia, F.J. & Gardner, T.W. 1994. Late Cenozoic flexural deformation of the middle United-States Atlantic passive margin. *Journal of Geophysical Research—Solid Earth*, **99**, 12143–12157.

Price, L.C. & Barker, C.E. 1985. Suppression of vitrinite reflectance in amorphous rich kerogen—a major unrecognized problem. *Journal of Petroleum Geology*, **8**, 59–84.

Roberts, A.M. & Holdsworth, R.E. 1999. Linking onshore and offshore structures: Mesozoic extension in the Scottish Highlands. *Journal of the Geological Society, London*, **156**, 1061–1064.

Rohrman, M. & van der Beek, P. 1996. Cenozoic postrift domal uplift of North Atlantic margins: an asthenospheric diapirism model. *Geology*, **24**, 901–904.

Stewart, S.A. 1996. Tertiary extensional fault systems on the western margin of the North Sea Basin. *Petroleum Geoscience*, **2**, 167–176.

Thomson, K., Underhill, J.R., Green, P.F., Bray, R.J. & Gibson, H.J. 1999. Evidence from apatite fission track analysis for post-Devonian burial and exhumation history of the northern Highlands, Scotland. *Marine and Petroleum Geology*, **16**, 27–39.

Underhill, J.R. 1991a. Implications of Mesozoic–Recent basin development in the Inner Moray Firth, UK. *Marine and Petroleum Geology*, **8**, 359–369.

Underhill, J.R. 1991b. Controls on Late Jurassic seismic sequences, Inner Moray Firth, UK North Sea: a critical test of a key segment of Exxon's original sea-level chart. *Basin Research*, **3**, 79–98.

Underhill, J.R. 1998. Jurassic. *In:* Glennie, K. (ed.) *Introduction to the Petroleum Geology of the North Sea*, *4th*. Blackwell Science, Oxford, 245–293.

Underhill, J.R. 2001. Controls on the genesis and prospectivity of Paleogene palaeogeomorphic traps, East Shetland Platform, UK North Sea. *Marine and Petroleum Geology*, **18**, 259–281.

Underhill, J.R. & Partington, M.A. 1993. Jurassic thermal doming and deflation in the North Sea: implications of sequence stratigraphic evidence. *In:* Parker, J.R. (ed.) *Petroleum Geology of Northwest Europe: Proceedings of the 4th Conference*. Geological Society, London, 337–345.

Received 18 October 2001; revised typescript accepted 21 May 2002.
Scientific editing by Haakon Fossen